

Carbon: The Soul of Future Nanoelectronics

Vijay K. Arora

Abstract Quantum transport in carbon allotropes emerging from graphene/graphite nanolayers is described. Nonequilibrium Arora's distribution function (NEADF) includes the energy gained/lost in a mean free path (mfp) in the presence of an electric field. It is shown to organize the randomness in equilibrium to streamlined motion in extreme nonequilibrium leading to saturation of drift velocity and the current. A simple tanh form is obtained that is strictly valid for nondegenerate statistics, but is extended to degenerate statistics by defining a degeneracy temperature. Ballistic transport where device length is smaller than the scattering-limited mfp is shown to degrade the mobility. Resistance quantum is obtained in 1D configuration that is generalized to give contact resistance and channel resistance. Magnetotransport in graphene is discussed to demonstrate the utilization of magnetic field in characterization and performance evaluation.

1 Introduction

Graphene, a single layer of graphite with carbon atoms arranged in a honeycomb lattice is a perfect 2D conductor. As Fig. 1 shows, graphene can form a 0D nanostructure as a nanometer-size fullerene molecule, a 1D carbon nanotube (CNT) made of rolled-up sheets of graphene; a 1D graphene nanoribbon (GNR) cutouts from a graphene sheet with a narrow width of high aspect ratio; 3D with graphene layer stacked as in a graphite. The stacks of GNRs or 2D nanolayers can transform to multilayer graphene each with unique properties.

Each atom at the corner of honeybee hexagon is a carbon atom with electronic configuration that is similar to silicon as both come from Group 4 of the Periodic Table. Carbon (${}_6\text{C}^{12}$) atom with 6 electrons has electronic configuration $1s^2 2s^2 2p^2$. It is a tetravalent material with four of its electrons in shell 2 and still able to

V.K. Arora (✉)

Department of Electrical Engineering and Physics, Wilkes University,
Wilkes-Barre PA 18766, USA
e-mail: vijay.arora@wilkes.edu

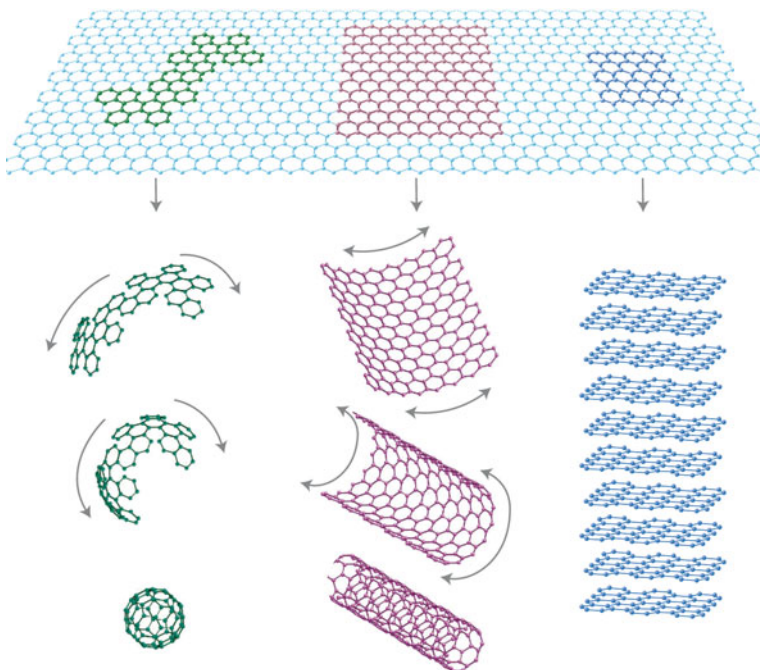


Fig. 1 Graphene sheet transforming to fullerene, carbon nanotube (CNT), graphene nanoribbon (GNR), and multilayer graphene each with unique properties. Copyright Macmillan Publishers Limited [4]

accommodate 4 more in 2p orbitals. However, carbon orbitals can hybridize because the s-orbital and p-orbitals of carbon's second electronic shell have very similar energies [1]. As a result, carbon can adapt to form chemical bonds with different geometries.

Graphene has many extraordinary electrical, mechanical, and thermal properties, such as high carrier mobility, ambipolar electrical field effect, tunable band gap, room temperature quantum Hall effect, high elasticity, and superior thermal conductivity. It is projected to be a material of scientific legend, comparable only to penicillin as a panacea. There is a modern adage: silicon comes from geology and carbon comes from biology. Cohesive band structure of graphene rolled into a CNT in a variety of chiral directions has recently been reported [2]. It is shown to exist in metallic and semiconducting states. Similarly GNR with narrow width are shown in three semiconducting modes with no metallic configuration [3]. All semiconducting states can be described with parabolic E-k relation with effective mass, while the effective mass for metallic state remains zero, as in graphene.

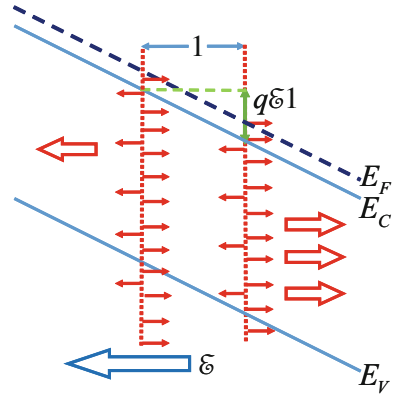
Quantum and ballistic transport offer a new outlook with the appearance of many outstanding properties of graphene and its allotropes [1]. Equilibrium carrier statistics with large number of stochastic carriers is the basis of any transport and is well established. However, nonequilibrium quantum transport based on the

Hamiltonian formulation is complex. One is easily lost in the computational maze of Monte Carlo experiments where myriad of parameters control the output. On the other hand, nonequilibrium Arora's distribution function (NEADF) [5] is distinctly simpler in its outlook with only the mean free path (mfp) as a parameter obtainable from low-field mobility that is always measured in any transport experiment. A new paradigm for characterization and performance evaluation of carbon allotropes is emerging from the application of NEADF to graphene and its allotropes. NEADF's unique feature is conversion of the stochastic carrier motion in equilibrium with no external influences into a streamlined one in a high-field-initiated extreme nonequilibrium for current to flow and get saturated. The mobility expressions are direct product of NEADF when limit to low-field domain is obtained. Similarly, the nondegenerate statistics is transformed to degenerate one by defining the degeneracy temperature to reveal higher energy in the degenerate state as the Fermi energy resides in one of the bands.

2 NEADF

NEADF is an outgrowth of the Fermi-Dirac distribution with the added energy lost/gained $q\vec{\mathcal{E}} \cdot \vec{\ell}_{o\infty} = q\mathcal{E}\ell_{o\infty} \cos \theta$ in and opposite to the electric field with $-1 \leq \cos \theta \leq +1$. The presence of $\cos \theta$ favors those electrons drifting opposite to $\vec{\mathcal{E}}$ as shown in Fig. 2. The velocity at any collision is stochastic with average magnitude equal to intrinsic velocity v_i that is thermal velocity in nondegenerate (ND) domain and Fermi velocity in degenerate domain. This intrinsic velocity is the Fermi velocity $v_{Fo} = 10^5$ m/s at Dirac point. The saturation current is $I_{sat} = n_3 q v_{sat} A_c(3D)$, $I_{sat} = n_2 q v_{sat} W(2D)$, $I_{sat} = n_1 q v_{sat}(1D)$, where $v_{sat} = v_{id}$ for a given dimensionality d (3, 2, or 1). Saturation is further lowered by an onset of quantum emission. The mathematical form of NEADF is given by [6]

Fig. 2 Left-right asymmetry in the electric-field direction



$$f(E, \mathcal{E}) = \frac{1}{1 + e^{\frac{E - (E_F + q\mathcal{E}\ell)}{k_B T}}} \quad (1)$$

The mfp ℓ , related to long-channel mfp $\ell_{o\infty}$, as modified by the quantum emission, is given by

$$\ell = \ell_{o\infty} \left(1 - e^{-\frac{\ell_Q}{\ell_{o\infty}}} \right) \quad (2)$$

with

$$\ell_Q = \hbar\omega_0(N_o + 1)/q\mathcal{E} \quad (3)$$

$$N_o = 1/(e^{\Delta_Q} - 1), \Delta_Q = \hbar\omega_o/k_B T \quad (4)$$

At any collision, the electron start from stochastic velocity directed at random. The component in and against electric field $\vec{\mathcal{E}}$ is affected. Those with intrinsic velocity directed in the +x direction (opposite to $\vec{\mathcal{E}}$) gain velocity $v_+ = v_i + q\mathcal{E}\tau_c$ and those directed towards -x direction decelerate with $v_- = -v_i + q\mathcal{E}\tau_c$, where $\tau_c \approx \ell_{o\infty}/v_i$ is the collision time. The average in a mfp results in net drift $v_D = q\mathcal{E}\tau_c/m^* = \mu_{o\infty}\mathcal{E}$ proportional to \mathcal{E} assuming equipartition ($n_+ = n_- = n/2$) of velocity until $v_- = 0$. As v_- turning point gets smaller than the mfp, anisotropy in the distribution sets in making $n_+ > n_-$. That is the initiation of unidirectional transport at the critical value $\mathcal{E}_c = v_i/\mu_{o\infty}$. The onset of quantum emission lowers the saturation velocity below v_i as $\ell_Q < \ell_{o\infty}$. In the extreme nonequilibrium $n_+ = n$ and $n_- = 0$ and carrier velocity vectors are unidirectional leading to saturation velocity and current.

3 Drift Response

Equilibrium 2D carrier concentration n_g in graphene is given by [5]

$$n_g = N_g \mathfrak{S}_1(\eta) \quad (5)$$

with

$$N_g = (2/\pi)(k_B T / \hbar v_F)^2 \quad (6)$$

$$\eta = (E_F - E_{Fo})/k_B T \quad (7)$$

$\mathfrak{S}_j(\eta)$ is the Fermi-Dirac integral (FDI) of order j [7, 8] with j = 1 for graphene. The linear carrier density of CNT is similarly described by

$$n_{CNT} = N_{CNT} \mathfrak{S}_{CNT}(\eta, e_g) \quad (8)$$

with $D_o = 4/\pi\hbar v_{Fo} = 1.93 \text{ eV}^{-1} \text{ nm}^{-1}$, $e_g = E_g/k_B T$. $N_{CNT} = D_o k_B T$ is the effective density of states. $\mathfrak{S}_{CNT}(\eta, e_g)$ is the CNT integral that can be evaluated numerically [2]. Equilibrium carrier statistics for GNR is similarly obtainable [3].

The drift response v_D to an applied electric field in a graphene nanolayer is the average of $v_{Fo} \cos \theta$ using the NEADF and density of states, resulting in

$$v_D/v_{Fo} = (1/2\pi u_g) \int_0^{2\pi} \cos \theta d\theta \mathfrak{S}_1(H(\theta)) \quad (9)$$

The reduced Fermi energy η is now a function of electric field and is evaluated from the normalization condition

$$u_g = (1/2\pi) \int_0^{2\pi} d\theta \mathfrak{S}_1(H(\theta)), \quad u_g = n_g/N_g \quad (10)$$

Here $H(\theta) = \eta - \delta \cos \theta$ is the electrochemical Fermi energy that is directional. A simplified version of (9) is obtained by substitution of $\cos \theta = \pm 1/2$ in $H(\theta)$ as distribution is split into $\pm x$ -direction. $\theta = -\pi/2$ to $+\pi/2$ is for $+x$ -direction and $\theta = +\pi/2$ to $+3\pi/2$ for $-x$ -direction. $\langle \cos \theta \rangle = \pm 1/d$ for an arbitrary dimensionality $d = 3, 2$, and 1 [9, 10]. With this substitution, the relative drift response of (9) is the same as difference of anisotropic carriers in an electric field as shown in Fig. 2. The drift response for 2D graphene is now obtained as

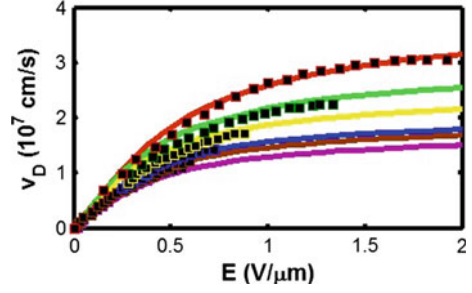
$$v_D = v_{Fo} \frac{\mathfrak{S}_1(\eta + \delta/2) - \mathfrak{S}_1(\eta - \delta/2)}{\mathfrak{S}_1(\eta + \delta/2) + \mathfrak{S}_1(\eta - \delta/2)} \quad (11)$$

where $n_{g\pm} = N_g \mathfrak{S}_1(\eta \pm \delta/2)$ is the carrier concentration with velocity vector component in the $\pm x$ direction with electric field in the $-x$ direction. The mobility expression follows naturally from (11) in the low-electric-field limit ($\delta \rightarrow 0$) and using $d\mathfrak{S}_j(\eta)/d\eta = \mathfrak{S}_{j-1}(\eta)$. The mobility expression is obtained as

$$\mu_{og} = \frac{q\ell v_{Fo}}{2k_B T} \frac{\mathfrak{S}_0(\eta_o)}{\mathfrak{S}_1(\eta_o)} \quad (12)$$

Here η_o is used in place of η to emphasize the fact that it is zero-field reduced Fermi energy. The mobility expression of (12) allows one to define ohmic degeneracy temperature T_{og} so mobility expression is re-written as

Fig. 3 Drift velocity v_D as a function of electric field \mathcal{E} at room temperature $T = 280$ K for $n_g/10^{16}\text{m}^{-2} = 1.6$ (top), 2.8, 4.2, 6.4, 8.6, and 10.3 (bottom). The solid line represents v_D from theory (11). The markers are the experimental data of [12]



$$\mu_{og} = \frac{q\ell v_{Fo}}{2k_B T_{og}}, \quad T_{og} = T \frac{\mathfrak{S}_1(\eta_o)}{\mathfrak{S}_o(\eta_o)} \quad (13)$$

Figure 3 shows the graphene's drift response to high electric field with solid lines obtained from (11) with the mfp extracted from (12) for the experimental data on mobility. The comments on this drift response appear in [11].

The drift response in a CNT can be similarly evaluated. For a semiconducting CNT, it does involve CNT integral, but for a metallic CNT, the drift response is similar to that of (11) with $\mathfrak{S}_1(\eta)$ replaced with $\mathfrak{S}_o(\eta)$. The mobility for a metallic MCNT is given by

$$\mu_{oMCNT} = \frac{q\ell v_{Fo}}{k_B T_{oMCNT}}, \quad T_{oMCNT} = T \frac{\mathfrak{S}_{-1}(\eta_o)}{\mathfrak{S}_o(\eta_o)} \quad (14)$$

The current response I to the applied voltage is given by

$$I = I_{sat} \frac{\mathfrak{S}_o(\eta + \delta_o) - \mathfrak{S}_o(\eta - \delta_o)}{\mathfrak{S}_o(\eta + \delta_o) + \mathfrak{S}_o(\eta - \delta_o)} \quad (15)$$

A simplification of (15) is possible if CNT degeneracy temperature of (14) is utilized. The thermal voltage $V_t = k_B T/q$ is now replaceable with $V_F = E_F/q$ in extreme degeneracy. This will make the current response temperature independent. The current response of (15) is now simplified to

$$I = I_{sat} \tanh(V/V_c) \quad (16)$$

where $V_c = (V_F/\ell_{o\infty})L$. The sublinear nature of I-V curves of Fig. 4 obtained from (16) requires distinction between direct ($R = V/I$) and incremental resistance ($r = dV/dI$). In the ohmic domain ($I = V/R_o$), $r_o = R_o = 40$ k Ω due to constant I-V slope. However, in the sublinear regime beyond $V = V_c$, distinction between R and r is a must. R and r over the complete regime, as obtained from (16), are given by

Fig. 4 The current response to the applied voltage in a metallic CNT

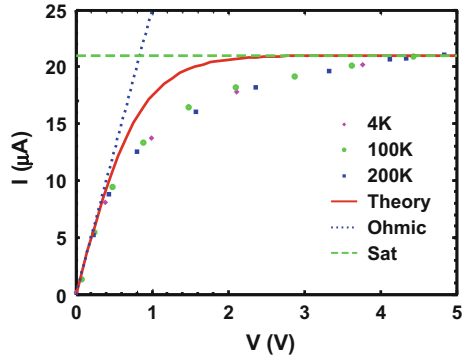
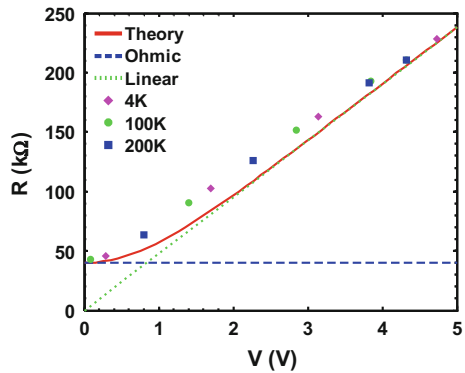


Fig. 5 The resistance as a function of applied voltage in an MCNT with ohmic resistance $R_o = 40 \text{ k}\Omega$



$$R = R_o(V/V_c) / \tanh(V/V_c) \quad (16)$$

$$r = R_o \cosh^2(V/V_c) \quad (17)$$

Figure 5 shows direct resistance as a function of voltage. The resistance approaches its ohmic value in the limit of low value of the voltage ($V < V_c$), but rises linearly with voltage in the high-voltage limit ($V \gg V_c$). The experimental data in Figs. 4 and 5 is obtained from [13]. The direct resistance R as a function of voltage is shown in Fig. 5. As the figure shows, the resistance converges to constant R_o as $V \rightarrow 0$, but rises linearly with voltage consistent with (16) as $\tanh(V/V_c) \approx 1$ when $V \gg V_c$.

4 Ballistic Transmission

The absence of electron scattering in a conducting channel with length below the scattering-limited mfp is technically called ballistic transmission. The absence of scattering is conjectured to give higher mobility and hence the interest in ballistic

transmission. Contrary to this belief, the experiments show resistance rising and mobility degrading even in the ohmic domain where high-field effects are negligible [14–16].

In a 1D CNT, just like in a 1D nanowire [9, 17], the product of velocity and density of states (DOS) is constant [18]. In fact that is the general property of any 1D system. Differential DOS ($2g_K/hv(E)dE$) between E and $E + dE$ in a CNT is inversely proportional to velocity $v(E)$ [2], where $g_K = 2$ is K-K' degeneracy in hexagonal k-space. Only half the electrons, as shown in Fig. 6 are transmitted ballistically from left to right. Backward reflection at $T = 0$ K is blocked due to Pauli Exclusion Principle that forbids transmission in occupied destination states. With probability of occupation unity at low temperatures, the current I is obtained by integrating $qv(E)(4/hv(E))dE$ from E_{FR} to E_{FL} with $E_{FL} - E_{FR} = qV$. The current is then $I = (4q^2/h)V$, giving quantum resistance $R_Q = h/4q^2$. The same paradigm applies to graphene nanoribbons (GNRs) which are also 1 D in nature.

At extremely undersized dimensions L smaller than the scattering-limited long-channel mfp $\ell_{o\infty}$ ($L < \ell_{o\infty}$), Arora et al. [14, 16, 19, 20] show the probabilistic nature of the collisions that give a finite probability for scattering even in short channels leading to non-unity ballisticity [16] that takes into account ballistic injection from the contacts. The length-limited ballistic ohmic mobility μ_{oL} is given by [16]

$$\mu_{oLCNT} = \mu_{o\infty CNT}(1 - e^{-L/\ell_B}) \quad (18)$$

The ballistic mfp $\ell_B = \ell_{o\infty}(v_{inj}/v_{Fo})$ differs from the traditional low-field (o) long-channel (∞) mfp $\ell_{o\infty}$ by a factor (v_{inj}/v_{Fo}) , where v_{inj} is the velocity of the injected carriers from the contacts. $\ell_B = \ell_{o\infty}$ as injection is limited to the Fermi velocity for a CNT. In the limit of $L \ll \ell_{o\infty}$, (18) coupled with (14) gives

$$\mu_{LCNT} \approx \frac{8qL}{n_{CNT}h} \quad (19)$$

The resistivity for a 1D metallic CNT is given by

$$\rho_{CNT} = \frac{1}{(n_{CNT}/2)q\mu_{LCNT}} = \frac{h}{4q^2} \frac{1}{L} \quad (20)$$

Fig. 6 A ballistic conductor of length L connected between two metallic reservoirs with shifted Fermi energy in the presence of an electric field $\mathcal{E} = V/L$ applied from right to left

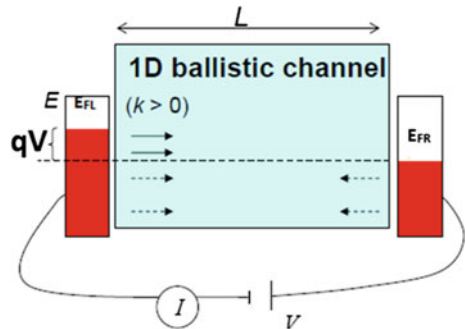
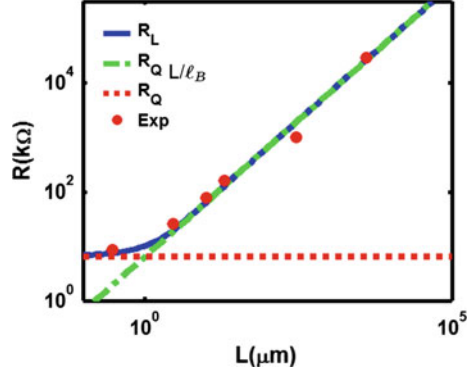


Fig. 7 The Resistance in a CNT as a function of channel length (solid line). The dotted line is applicable for long-channel behavior. The flat line is the ballistic quantum resistance



The quantum resistance R_Q now follows naturally from (20)

$$R_Q = \rho_{CNT} L = \frac{h}{4q^2} = 6.453 \text{ k}\Omega \quad (21)$$

The length-limited resistance now follows the pattern

$$R/R_Q = 1/T_r = (L/\ell_B)/(1 - e^{-L/\ell_B}) \quad (22)$$

where T_r is the transmission that is unity in the limit $L \rightarrow 0$. Figure 7 gives Resistance as a function of length, converging to R_Q as $L \rightarrow 0$ and a linear function of L as $L \gg \ell_B$. This type of scaling and electron mfp has been demonstrated by Purewal et al. [21] in a number of experiments on metallic and semiconducting nanotubes.

5 Magnetotransport

The appearance of quantum Hall effect in graphene is quite miraculous with the application of a magnetic field. Figure 10 is display of the doubly degenerate K-K' band structure of graphene. However, this Dirac point may be lifted or depressed due to quantum effects, creating a bandgap as when a magnetic field B is applied normal to the graphene layer. The trajectory of an electron (or hole) is a circle in a magnetic field as is well known. The circumference of the trajectory must contain integral number of de Broglie waves, i.e., $2\pi R = n\lambda_D = n(2\pi/k)$ resulting in $k_n = n/R_n$. As shown in Fig. 9, the magnetic force $qv_{Fo}B = \hbar kv_{Fo}/R_n$. Quantized radius $R_n = (n\hbar/qB)^{1/2}$ is obtained when $k_n = n/R_n$ is utilized to eliminate k_n , which is the same expression as for a parabolic semiconductor. In fact, negative values of n can be attributed to hole transport. It is appropriate to take $|n|$ in the expression for the radius (Fig. 8).

Fig. 8 2D graphene lattice with K-K' Dirac cone displayed. The application of magnetic field introduces a bandgap

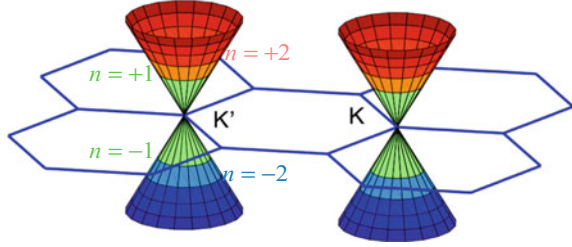


Fig. 9 Electron (hole) trajectory in a magnetic field B and associated centripetal force

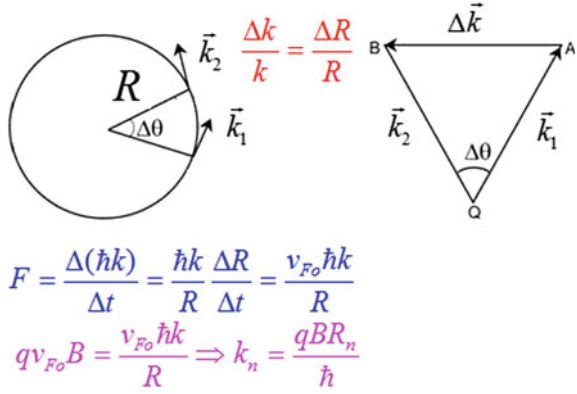
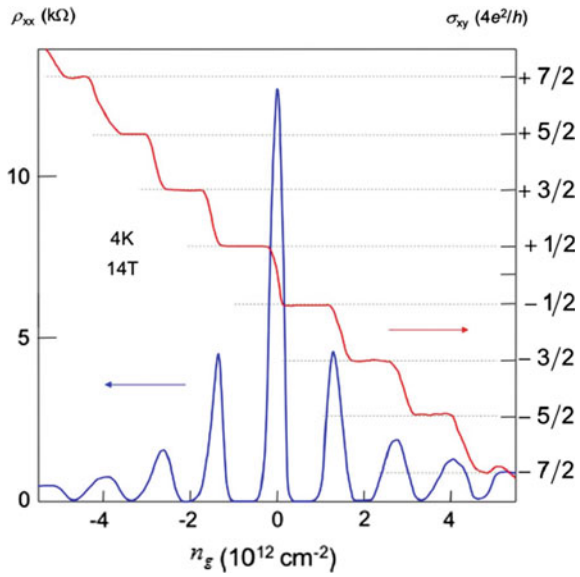


Fig. 10 Quantum Hall plateaus and vanishing resistivity in the localized domain [4, 22, 23]



The energy spectrum in a magnetic field now emerges as

$$E_n - E_{\pm o} = \pm \hbar v_{Fo} k_n = \pm \hbar v_{Fo} \frac{n}{R_n} = \pm v_{Fo} \sqrt{2nq\hbar B} \quad (23)$$

2D carrier density now splits into a number of quantum discs in k -space. The carrier concentration in each level is given by graphene statistics [1]

$$n_{gn} = N_g \mathfrak{S}_1(\eta) \approx (2/\pi)(k_B T / \hbar v_F)^2 (\eta^2/2) \quad (24)$$

with $\eta = (E_F - E_{+o})/k_B T$. When electrons are localized in a quantum disc, the Fermi level resides there with $(E_F - E_{+o}) = v_{Fo} \sqrt{2nq\hbar B}$ for $n > 1$. $K = 0$ in the lowest state as no quantum states exist below this energy, therefore $n_{g1} = 1/2$ for a singular quantum state as DOS contains both k_+ and k_- . Collectively, when executed

$$n_{gn} = \frac{4qB}{h} \left(n - \frac{1}{2} \right) \quad n = 1, 2, 3, \dots \quad (25)$$

The quantum energy reducing to half of that in a regular level is a direct result of Landau gauge in which the wavefunction is that of a harmonic oscillator. In parabolic semiconductors, it gives $1/2\hbar\omega_c$ due to potential energy of the oscillator, whereas the kinetic energy is quantized as $n\hbar\omega_c$ giving total energy $(n - 1/2)\hbar\omega_c$.

The components of resistivity ρ and conductivity σ are related by

$$\rho_{xx} = \frac{\sigma_{xx}}{\sigma_{xx}^2 + \sigma_{xy}^2} \quad \rho_{xy} = \frac{\sigma_{xy}}{\sigma_{xx}^2 + \sigma_{xy}^2} \quad (26)$$

where ρ_{xx} (σ_{xx}) is the longitudinal component and ρ_{xy} (σ_{xy}) is the Hall component. When the chemical potential (Fermi energy) is inside a region of localized states, the longitudinal conductivity vanishes $\sigma_{xx} = 0$ as electrons cannot freely move because all states are occupied. On the other hand, when the chemical potential is in a region of delocalized states, not in a quantized level, $\sigma_{xx} \neq 0$ and σ_{xy} varies continuously. In the localized domain

$$\rho_{xx} \approx 0 \quad (27)$$

$$\rho_{xy} \approx \frac{1}{\sigma_{xy}} = \frac{B}{qn_g} = \frac{h}{4q^2} \frac{1}{\left(n - \frac{1}{2}\right)} \quad n = 1, 2, 3, \dots \quad (28)$$

Figure 10 gives quantum plateaus as well as vanishing resistivity [4, 22, 23]. At the point where Hall plateau appears, the resistivity drops to zero.

6 Conclusions

The NEADF is unique for high-field applications as it seamlessly makes a transition from ohmic domain to nonohmic domain. The drive to reduce the size below the scattering-limited mfp to enhance transport behavior does not appear to be appropriate [7, 24–27]. That is perhaps the reason that observed experimental resistance of $40.0\text{ k}\Omega$ as observed by Yao et al. [13] exceeds its ballistic value for $1\text{-}\mu\text{m}$ resistor. In fact, Greenberg and Del Alamo [24] have demonstrated that resistance surge in the parasitic regions degrades the performance of an InGaAs transistor. To sum it up, explorations of new physical phenomena on this length scale require the contributions from many different fields of science and engineering, including physics, chemistry, biology, materials science, and electrical engineering.

References

1. P.H.S. Wong, D. Akinwande, *Carbon Nanotube and Graphene Device Physics* (Cambridge University Press, Cambridge, 2011)
2. V.K. Arora, A. Bhattacharyya, Cohesive band structure of carbon nanotubes for applications in quantum transport. *Nanoscale* **5**, 10927–10935 (2013)
3. V.K. Arora, A. Bhattacharyya, Unified bandgap engineering of graphene nanoribbons. *Physica status solidi (b)*. **251**(11) (2014)
4. A.K. Geim, K.S. Novoselov, The rise of graphene. *Nat. Mater.* **6**, 183–191 (2007)
5. V.K. Arora, M.L.P. Tan, C. Gupta, High-field transport in a graphene nanolayer. *J. Appl. Phys.* **112**, 114330 (2012)
6. V.K. Arora, *Nanoelectronics: Quantum Engineering of Low-Dimensional Nanoensembles* (CRC Press/Taylor and Francis Group, USA, 2015)
7. V.K. Arora, M.L.P. Tan, in *High-Field Transport in Graphene and Carbon Nanotubes, presented at the International Conference on Electron Devices and Solid State Circuits 2013 (EDSSC2013), IEEEExplore Digital Library*, Hong Kong Polytechnic University, 2013
8. V.K. Arora, *Nanoelectronics: Quantum Engineering of Low-Dimensional Nanoensemble* (Wilkes University, Wilkes-Barre, 2013)
9. V.K. Arora, D.C.Y. Chek, M.L.P. Tan, A.M. Hashim, Transition of equilibrium stochastic to unidirectional velocity vectors in a nanowire subjected to a towering electric field. *J. Appl. Phys.* **108**, 114314–114318 (2010)
10. V.K. Arora, *Quantum Nanoengineering* (Wilkes University, Wilkes-Barre, PA, 2012)
11. M.L.P. Tan, V.K. Arora, “Comment on “Theoretical analysis of high-field transport in graphene on a substrate”. [*J. Appl. Phys.* 116, 034507 (2014)],” *J. Appl. Phys.* **116** (2014)
12. V.E. Dorgan, A. Behnam, H.J. Conley, K.I. Bolotin, E. Pop, High-field electrical and thermal transport in suspended graphene. *Nano Lett.* **13**, 4581–4586 (2013)
13. Z. Yao, C.L. Kane, C. Dekker, High-field electrical transport in single-wall carbon nanotubes. *Phys. Rev. Lett.* **84**, 2941–2944 (2000)
14. V.K. Arora, M.S.Z. Abidin, M.L.P. Tan, M.A. Riyadi, Temperature-dependent ballistic transport in a channel with length below the scattering-limited mean free path. *J. Appl. Phys.* **111**, 054301, 1 Mar 2012
15. V.K. Arora, M.S.Z. Abidin, S. Tembhurne, M.A. Riyadi, Concentration dependence of drift and magnetoresistance ballistic mobility in a scaled-down metal-oxide semiconductor field-effect transistor, *Appl. Phys. Lett.* **99**, 063106–063106–3 (2011)

16. M.A. Riyadi, V.K. Arora, The channel mobility degradation in a nanoscale MOSFET due to injection from the ballistic contacts. *J. Appl. Phys.* **109**, 056103 (2011)
17. P. Yang, R. Yan, M. Fardy, Semiconductor nanowire: What's next? *Nano Lett.* **10**, 1529–1536 (2010)
18. H.C. Chin, A. Bhattacharyya, V.K. Arora, Extraction of nanoelectronic parameters from quantum conductance in a carbon nanotube. *Carbon* **76**, 451–454 (2014)
19. V.K. Arora, “*Ballistic transport in nanoscale devices*,” presented at the *MIXDES 2012: 19th International Conference MIXED Design of Integrated Circuits and Systems* (Wasaw, Poland, 2012)
20. V.K. Arora, M.S.Z. Abidin, M.L.P. Tan, M.A. Riyadi, Temperature-dependent ballistic transport in a channel with length below the scattering-limited mean free path. *J. Appl. Phys.* **111**, 1 Mar 2012
21. M.S. Purewal, B.H. Hong, A. Ravi, B. Chandra, J. Hone, P. Kim, Scaling of resistance and electron mean free path of single-walled carbon nanotubes. *Phys. Rev. Lett.* **98**, 186808, 4 May 2007
22. K.S. Novoselov, S.V. Morozov, T.M.G. Mohinddin, L.A. Ponomarenko, D.C. Elias, R. Yang, I.I. Barbolina, P. Blake, T.J. Booth, D. Jiang, J. Giesbers, E.W. Hill, A.K. Geim, Electronic properties of graphene. *Physica Status Solidi B-Basic Solid State Phys.* **244**, 4106–4111 (2007)
23. A.H. Castro Neto, F. Guinea, N.M.R. Peres, K.S. Novoselov, A.K. Geim, The electronic properties of graphene. *Rev. Mod. Phys.* **81**, 109–162 (2009)
24. D.R. Greenberg, J.A.d. Alamo, Velocity saturation in the extrinsic device: a fundamental limit in HFET's. *IEEE Trans. Electron. Devices* **41**, 1334–1339 (1994)
25. V.K. Arora, “*Quantum Transport in Nanowires and Nanographene*,” presented at the *28th International Conference on Microelectronics (MIEL2012)*, Nis, Serbia (2012)
26. T. Saxena, D.C.Y. Chek, M.L.P. Tan, V.K. Arora, Microcircuit modeling and simulation beyond Ohm's law. *IEEE Trans. Educ.* **54**, 34–40 (2011)
27. M.L.P. Tan, T. Saxena, V. Arora, Resistance blow-up effect in micro-circuit engineering. *Solid-State Electron.* **54**, 1617–1624 (2010)

Recent Trends in Materials and Devices

Proceedings ICRTMD 2015

Jain, V.K.; Rattan, S.; Verma, A. (Eds.)

2017, XXVII, 547 p. 315 illus., 226 illus. in color.,

Hardcover

ISBN: 978-3-319-29095-9